Physics and Chemistry of Minerals (2019) 46:727–741
https://doi.org/10.1007/s00269-019-01034-0

ORIGINAL PAPER

Redefinition and crystal chemistry of samarskite-(Y), $YFe^{3+}Nb_2O_8$: cation-ordered niobate structurally related to layered double tungstates

Sergey N. Britvin[1,2] · Igor V. Pekov[3] · Maria G. Krzhizhanovskaya[1] · Atali A. Agakhanov[4] · Bernd Ternes[5] · Willi Schüller[6] · Nikita V. Chukanov[7]

Received: 5 February 2019 / Accepted: 8 April 2019 / Published online: 23 April 2019
© Springer-Verlag GmbH Germany, part of Springer Nature 2019

Abstract

Samarskite-(Y), the mineral known for almost 180 years only in metamict (X-ray amorphous) state, was found as non-metamict crystals in sanidinites of the Laach Lake (Laacher See), Eifel volcanic region, Germany. The crystal structure has been solved for the first time and refined to $R_1 = 1.1\%$ based on 838 observed [$I > 2\sigma(I)$] independent reflections. Samarskite-(Y) is monoclinic, $P2/c$, a 9.8020(8), b 5.6248(3), c 5.2073(4) Å, β 93.406(4)°, V 286.59(4) Å^3, $Z = 2$. The empirical formula (calculated on 8 O *apfu*) is $\left[\left(Y_{0.25}Ln_{0.18}\right)_{\Sigma 0.43}Th_{0.37}U^{4+}_{0.13}Ca_{0.03}\right]_{\Sigma 0.96}\left(Fe^{3+}_{0.73}Mn^{2+}_{0.18}\right)_{\Sigma 0.91}\left(Nb_{1.85}Ti_{0.06}Zr_{0.06}Ta_{0.03}W_{0.02}\right)_{\Sigma 2.02}O_8$. Samarskite-(Y) from the type locality, the Blyumovskaya Pit, Ilmeny Mountains, South Urals, Russia, was studied for comparison; electron microprobe data showed the same species-defining constituents and stoichiometry: $\left[\left(Y_{0.34}Ln_{0.20}\right)_{\Sigma 0.54}U^{4+}_{0.42}Th_{0.03}\right]_{\Sigma 0.99}\left(Fe^{3+}_{0.86}Mn^{2+}_{0.08}\right)_{\Sigma 0.94}\left(Nb_{1.14}Ta_{0.70}Ti_{0.15}\right)_{\Sigma 1.99}O_8$. Samarskite-(Y) is the first example of cation-ordered niobate structurally related to layered double tungstates AMW_2O_8, the compounds used as luminophors and active media in solid-state lasers. The pseudo-layered framework of the mineral can be derived from that of wolframite via substitution of W for Nb, whereas each second [FeO_6] layer is replaced by [YO_8] one. The resulting sequence of layers can be expressed as -[AO_8]-[BO_6]-[MO_6]-[BO_6]- leading to the formula AMB_2O_8 in which A = Y, *Ln*, Th, U^{4+}, Ca; M = Fe^{3+}, Mn^{2+}; and B = Nb, Ta, Ti. The end-member formula of samarskte-(Y) is $YFe^{3+}Nb_2O_8$ (approved by the Commission on New Minerals, Nomenclature and Classification, International Mineralogical Association, memorandum 90-FH/18).

Keywords Samarskite · Niobate · Tantalate · Double tungstates · Crystal structure · Rare earths · Pegmatite · Metamict state · Phase transitions

Introduction

Samarskite-(Y) is one of the legendary, earliest known rare-earth minerals. Three new elements, samarium (Lecoq de Boisbaudran 1879), gadolinium (Marignac 1880; Lecoq de Boisbaudran 1886) and europium (Demarçay 1901) have

Electronic supplementary material The online version of this article (https://doi.org/10.1007/s00269-019-01034-0) contains supplementary material, which is available to authorized users.

✉ Sergey N. Britvin
sergei.britvin@spbu.ru

[1] Department of Crystallography, Institute of Earth Sciences, St. Petersburg State University, Universitetskaya Nab. 7/9, 199034 St. Petersburg, Russia

[2] Nanomaterials Research Center, Kola Science Center, Russian Academy of Sciences, Fersman Str. 14, 184200 Apatity, Russia

[3] Faculty of Geology, Moscow State University, Vorobievy Gory, 119991 Moscow, Russia

[4] Fersman Mineralogical Museum, Russian Academy of Sciences, Leninskiy Prospect, 18-2, 119071 Moscow, Russia

[5] Bahnhofstrasse 45, 56727 Mayen, Germany

[6] Im Straußenpesch 22, 53518 Adenau, Germany

[7] Institute of Problems of Chemical Physics, Russian Academy of Sciences, 142432 Chernogolovka, Moscow Region, Russia

been discovered in this mineral. Samarskite has been first described by Rose (1839) under the name "Uranotantal" from the open pit #50 (also known as the Blyumovskaya Pit) at the Ilmeny Mountains, South Urals, Russia. Later on (Rose 1847), the mineral was named Samarskite, in honor for V.E. Samarsky-Bykhovets, a chief of Russian Corps of Mining Engineers who had supplied the specimens for the study. The history of discovery and early studies of samarskite-(Y) were reviewed by Pekov (1998) and Polyakov (2000). Samarskite-(Y) is a typical accessory mineral in NYF (niobium–yttrium–fluorine) pegmatites and their parent granites (Černý et al. 2012; Dill 2015); therefore, variations of its chemical composition were thoroughly studied (e.g., Cassedanne et al. 1985; Hanson et al. 1998; Ercit 2005; Uher et al. 2009; Papoutsa and Pe-Piper 2013; Pieczka et al. 2014). However, the crystal structure of the mineral remained unsolved because samarskite-(Y) occurs in metamict state, i.e., X-ray amorphous due to structural damage caused by α-decay-self-irradiation (Ewing 1975). Other minerals considered as members of the samarskite group were found to be metamict as well: yttrotantalite-(Y), $(Y,U,Fe)(Ta,Nb)O_4$ (Brøgger 1906; Palache et al. 1944); ishikawaite, $(U,Fe,Y)NbO_4$ (Kimura 1922); calciosamarskite, $(Ca,Fe,Y)(Nb,Ta,Ti)O_4$ (Ellsworth 1928); and samarskite-(Yb), $YbNbO_4$ (Simmons et al. 2006). The first experiment aimed at restoring crystalline state of samarskite via annealing (Komkov 1965) showed that unit-cell metrics of the annealed mineral closely relate to those of $ScNbO_4$ (Keller 1962), the compound isostructural to wolframite $(Fe,Mn)WO_4$. Further studies (Sugitani et al. 1984, 1985; Hanson et al. 1999; Simmons et al. 2006; Tomašić et al. 2010) revealed the consecutive formation of orthorhombic (low-temperature) and monoclinic (high-temperature) oxide phases upon annealing of metamict samarskite. However, the crystal structures of obtained oxides could not be determined. Because of persistent uncertainties, the chemical formula of samarskite-(Y) is currently accepted by International Mineralogical Association in the form of ABO_4 where $A = (Y,Ln,Ca,Fe,U)$ and $B = (Nb,Ti,Ta)$ (Hanson et al. 1999).

In the course of mineralogical research of the Eifel volcanic region, Rhineland-Palatinate, Germany, the co-authors of the present paper (W.S. and B.T.) have found well-formed samarskite-(Y) crystals in the voids of sanidinite rocks of the Laach Lake (Laacher See in German) paleovolcano. This occurrence was briefly described by Engelhaupt and Schüller (2015). Since our previous studies showed that commonly metamict U- and Th-bearing minerals occur in the Eifel volcanic rocks in the non-metamict state (Chukanov et al. 2013, 2014), a single crystal of samarskite-(Y) has been selected for the aims of the present study. It was found that the mineral is non-metamict and possesses crystal structure derived from that of wolframite $(Fe,Mn)WO_4$. Namely, samarskite-(Y) is the first example of cation-ordered niobate related to a structural family of layered double tungstates (double wolframites) AMW_2O_8. These compounds, as well as their molybdate counterparts, are used as luminophors and active media in solid-state lasers (Pollnau et al. 2007; Zharikov et al. 2009; Lagatsky et al. 2010), whereas isostructural fluorovanadates are considered as attractive materials for Na-ion batteries (Donakowski et al. 2013).

It is noteworthy that although studies of samarskite-(Y) cover numerous localities worldwide, the reliable data on the mineral from the type locality, the Blyumovskaya Pit, are rather limited. It is obvious that the lack of proven information on the chemical composition of the type material resulted in the emergence of conclusions which doubt samarskite-(Y) as a distinct mineral species (Capitani et al. 2016). To ascertain the questions raised in the work by Capitani et al. (2016), we undertook a revision of samarskite-(Y) from the type locality, including electron microprobe, thermal and powder X-ray diffraction (XRD) studies. Like the non-metamict crystal from the Laacher See, the fully metamict mineral from the type locality demonstrates the same species-defining constituents and perfectly fulfils the stoichiometry of cation-ordered samarskite corresponding to $YFe^{3+}Nb_2O_8$ end-member. We herein provide the results of comparative study of samarskite-(Y) from both localities and discuss its relationships with synthetic double tungstates and closely related structures of wolframite and wodginite group minerals. The results of the present work have been approved by the Commission on New Minerals, Nomenclature and Classification, International Mineralogical Association (voting proposal 18-J; Memorandum 90-FH/18 of 05 December 2018) leading to the end-member formula of samarskite-(Y) $YFe^{3+}Nb_2O_8$.

Origin of the specimens

Laacher See

The Laacher See is one of about hundred Quaternary eruptive sites exposed at the East Eifel volcanic field in Central Rhineland (Bräuer et al. 2013). The effusive rocks of the Laacher See are outcropped in the old known *In den Dellen* (*Zieglowski*) quarry (50°23′35″N, 7°17′12″E) where they are represented by phonolites and a variety of pyroclastic tuffs enriched in xenoliths of carbonatites, syenites, glasses and sanidinites (Engelhaupt and Schüller 2015). The onset of the Laacher See eruptive event has been determined with a high precision (12916-year BP, Baales et al. 2002) indicative that it is the youngest volcano in the East Eifel area. One of remarkable mineralogical features of the Laacher See sanidinites is a variety of accessory minerals containing uranium and thorium. Because of youthful age of their formation, many of commonly metamict U- and Th-bearing

phases occur therein in crystalline state (Della Ventura et al. 2000; Kolitsch et al. 2012; Chukanov et al. 2012a, b, 2013, 2014). Samarskite-(Y) occurs inside millimeter-sized cavities of sanidinite where it forms sword-like crystals up to 0.3 mm in size flattened on {100}, with subordinate development of other faces (Fig. 1a). The crystal habit is well consistent with that of samarskite-(Y) from the type locality (Grigor'ev 1945; Polyakov et al. 1980; Polyakov 2000; Popov et al. 2007). The mineral is associated with sanidine, hematite, haüyne and phlogopite. Samarskite-(Y) possesses black color with brownish tint and strong resinous luster on broken surface. In the very thin grains (< 20 μm), the mineral is transparent and possesses reddish-brown color. Samarskite-(Y) is a rare mineral at the Laacher See. A single crystal, with the dimensions 0.25 × 0.15 × 0.05 mm, has been selected for the present study.

The Blyumovskaya Pit

The type locality for samarskite-(Y) is an open Pit #50 also known as the Blyumovskaya Pit. It was named after the mining engineer F.F. Blyum who founded the mine in 1835 (Pekov 1998). It is located at the southern part of the Ilmeny Mountains, South Urals, Russia (55°1′1″N, 60°11′35″E) and nowadays belongs to the Ilmen Nature Reserve. The pit exposes large differentiated albite–amazonite pegmatite vein (~ 150 m long, ~ 5 m wide) cross-cutting amphibolites and gneisses of 290–240 Ma age (Popov and Popova 2006). It was operated for gem-quality topaz and aquamarine since 1835 till 1843. The albitized zone of a pegmatite is enriched in accessory minerals including zircon, monazite-(Ce), columbite-(Fe), aeschynite-(Ce), allanite-(Ce), fergusonite-(Y), etc. Samarskite-(Y) is a common mineral in this zone where it occurs as prismatic to flattened crystals reaching up a few centimeters in size (Polyakov 2000; Popov et al. 2007). The mineral was a subject of special mining as a potential source of radium in 1911–1917 with a total recovered amount of ~ 15 kg (Popov and Popova 2006). A few millimeter-sized black grains of typical, visually unaltered samarskite-(Y) from this locality were picked up from the specimen #ST6333 (Fig. 1b) kindly provided for the present study by the Fersman Mineralogical Museum of Russian Academy of Sciences, Moscow.

Samples and methods

Sample labeling

The following labels are hereinafter used for the studied samples. LS: as-collected crystal of samarskite-(Y) from the Laacher See. BP: grains of untreated metamict samarskite-(Y) from the type locality, the Blyumovskaya Pit. LS-1100: crystal fragment of LS annealed at 1100 °C (see the thermal experiment T1 in the "Thermal analysis" below). BP-700: grains of BP heated to 700 °C (the thermal experiment T3). BP-1100: grains of BP annealed at 1100 °C (the thermal experiment T4).

Electron microprobe study

A ~ 100 μm crystal fragment of LS and ~ 1 mm grain of BP were embedded into epoxy resin, polished and coated with carbon film. Electron microprobe data were obtained by

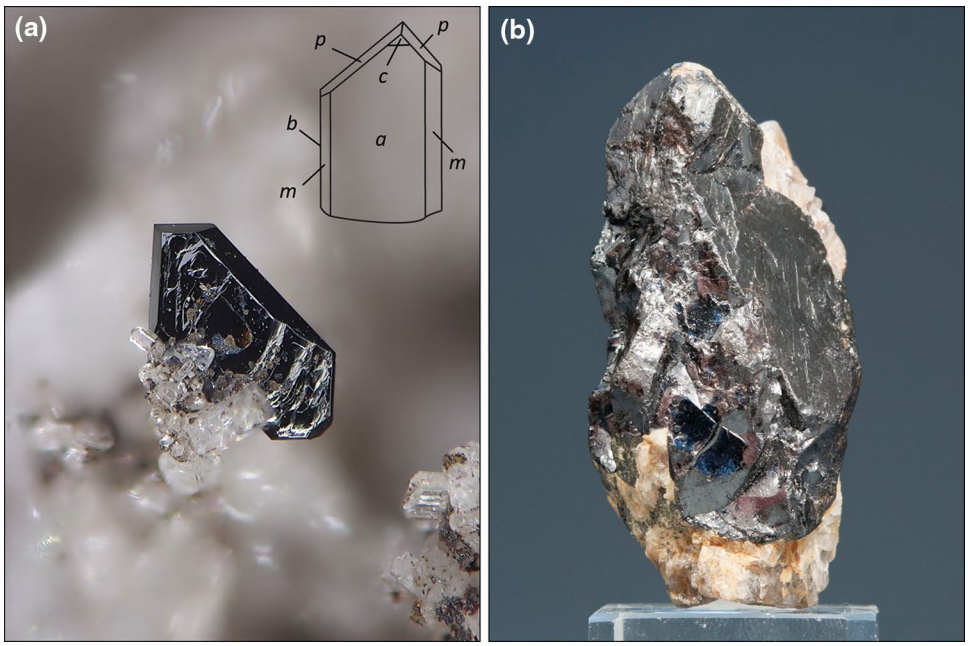

Fig. 1 Samarskite-(Y). **a** Crystal of samarskite-(Y) in the cavity of sanidinite, the Laacher See. Horizontal field of view: 0.5 mm. Photo: Willi Schüller. The top-right inset shows principal forms of the crystal labelled according to Polyakov et al. (1980), in monoclinic setting: *a*, {100}; *b*, {010}; *c*, {101}; *m*, {110}; and *p*, {111}. **b** Samarskite-(Y) from the Blyumovskaya Pit used in this study. Fragment of a single crystal intergrown with quartz and albite. Specimen height 7 cm. Courtesy of Fersman Mineralogical Museum, Russian Academy of Sciences (specimen #ST6333, photo: M.M. Moiseev)

means of a JEOL Superprobe JCXA-733 instrument. The grains were first examined in BSE mode and checked for elemental composition using energy-dispersive spectrometer. Quantitative analyses were performed in wavelength-dispersive mode under accelerating voltage of 15 kV, beam current 20 nA and beam diameter 3 μm. The following standards were used (analytical lines are given in parentheses): phosphates MPO_4 for *Ln* and Y (*L*α for Y, La, Ce, Gd, Tb, Tm and Yb; *L*β for Pr, Nd, Sm, Eu, Dy, Ho, Er and Lu); wollastonite (Ca*K*α); magnetite (Fe*K*α); ilmenite (Ti*K*α); $MnWO_4$ (Mn*K*α, W*M*α); $NaNbO_3$ (Nb*L*α); zircon (Zr*L*α); Ta (Ta*M*α); UO_2 (U*M*β) and ThO_2 (Th*M*α). Other elements were found below detection limits. The data obtained were recalculated using conventional *ZAF* correction.

Thermal analysis

These studies were aimed at (1) checking for thermal stability of crystalline samarskite-(Y) and (2) investigation of phase transformations of the metamict mineral. The studies were carried out using a Netzsch STA449F3 differential scanning calorimeter. Pt crucibles and dynamic argon atmosphere (99.9998% Ar, 50 mL/min flow rate) were used in all experiments. The program of the first thermal experiment (T1) involved annealing of 50 × 100 μm crystal fragment of LS and included three stages: (1) heating up to 1100 °C at the ramp rate of 10 °C/min; (2) annealing the crystal at 1100 °C for 36 h; (3) cooling down to 30 °C at the rate of 10 °C/min; the resulting sample is LS-1100. The second experiment (T2) was aimed at obtaining standard DSC and TG curves from ~ 4 mg of powdered sample of BP (heating rate of 10 °C/min to 1100 °C). The program of the third experiment (T3) included heating of ~ 5 mg of coarse-grained BP to 700 °C (10 °C/min) and cooling it down to 30 °C (20 °C/min); the resulting sample is BP-700. The fourth experiment (T4) involved annealing of separate batch of ~ 5 mg of coarse-grained BP and included three stages: (1) heating up to 1100 °C at the ramp rate of 10 °C/min; (2) annealing the sample at 1100 °C for 20 h; (3) cooling down to 30 °C at the rate of 10 °C/min; the resulting sample is BP-1100.

Single-crystal X-ray diffraction

The studies of LS and LS-1100 were carried out using Bruker Kappa APEX DUO and Bruker Smart APEX II CCD diffractometers at the room temperature. Data collection and reduction procedures (integration, absorption correction, scaling and setting up initial *SHELX* files) were performed using APEXII and SAINT software (Bruker 2003). The crystal structure of both LS and LS-1100 has been solved and refined using *SHELXT* and *SHELXL* suite of programs (Scheldrick 2015) and Olex2 software (Dolomanov et al. 2009). Data collection and structure refinement details are summarized and discussed in the X-ray crystallography and crystal structure section. The extended structural data for LS and LS-1100 are provided in the attached CIF file.

Powder X-ray powder diffraction

The crystal fragments of LS and LS-1100 used for structure solution were subsequently ground for the powder diffraction studies. The latter were carried out using Rigaku RAXIS Rapid II diffractometer (curved image plate, Debye–Scherrer geometry, $r = 127.4$ mm, Co*K*α, rotating anode with microfocus optics, 40 kV, 15 mA, exposure 15 min). Data conversion from the images to XY profiles was performed by means of osc2xrd program (Britvin et al. 2017). Pattern indexing and cell parameters refinement was performed by full-profile Rietveld fitting using Bruker Topas v.5.0 software (Bruker 2014). Full sets of powder XRD data for LS and LS-1100 are given in Supplementary materials (Table S1). XRD patterns of BP-700 and BP-1100 were obtained using Rigaku Ultima IV diffractometer (Cu*K*α, 40 kV, 30 mA, Bragg–Brentano geometry, $r = 285$ mm, linear PSD detector, divergence slit DS = 0.5 mm, 2Θ range 5°–100° at the scan step of 0.02°, exposure 18 h). Structure refinement and quantitative phase analysis of annealing products of metamict samarskite-(Y) (samples BP-700 and BP-1100) were performed by full-profile Rietveld fitting. The obtained results were processed with Bruker TOPAS V.5.0 software (Bruker 2014) employing 12-parameter Chebyshev polynomial for background simulation and Pearson VII profile-shape function.

Results and discussion

Chemical composition

Examination of polished sections of samarskite-(Y) from both the Laacher See and the Blyumovskaya Pit in BSE-EDX mode revealed compositional homogeneity of studied samples. Besides, thermogravimetric analysis of BP showed weight loss below 0.1 wt% upon annealing to 1100 °C indicating that BP does not contain chemically significant amount of water (experiment T2; Fig. S1 in Supplementary material). The electron microprobe data are given in Table 1. It can be seen that the chemical composition of samarskite-(Y) from both localities perfectly fulfils the stoichiometry AMB_2O_8 where *A* = Y, *Ln*, Th and U; *M* = Fe and Mn, *B* = Nb, Ta, W, Zr and Ti. In both samples Y, Fe and Nb are dominant, i.e., species-defining constituents in the *A*, *M* and *B* sites, respectively. The trivalent state of iron in LS is validated by bond-valence calculations (see the next section) and consistent with strongly oxidizing conditions of formation (Chukanov et al. 2014): the mineral is closely associated

Table 1 Chemical composition of samarskite-(Y) from the Laacher See (LS) and the Blyumovskaya Pit (BP) studied in this work

Constituent	LS[a]		BP[b]		Cation	Formula amount[c]	
	Wt%	Range	Wt%	Range		LS	BP
CaO	0.36	0.26–0.47	bdl		Ca	0.03	
Y_2O_3	5.30	5.02–5.75	6.42	5.88–6.80	Y	0.25	0.34
La_2O_3	0.18	0.00–0.37	0.07	0.00–0.36	La	0.01	< 0.01
Ce_2O_3	0.88	0.74–0.98	0.22	0.00–0.49	Ce	0.03	0.01
Pr_2O_3	0.12	0.00–0.72	0.09	0.00–0.16	Pr	< 0.01	< 0.01
Nd_2O_3	0.66	0.42–1.18	0.29	0.18–0.43	Nd	0.02	0.01
Sm_2O_3	0.34	0.00–0.61	0.49	0.14–0.98	Sm	0.01	0.02
Eu_2O_3	0.15	0.00–0.54	0.12	0.00–0.24	Eu	< 0.01	< 0.01
Gd_2O_3	0.48	0.00–0.87	0.48	0.17–0.77	Gd	0.01	0.02
Tb_2O_3	bdl		0.10	0.08–0.40	Tb	< 0.01	< 0.01
Dy_2O_3	1.35	0.72–1.97	1.59	1.29–1.92	Dy	0.04	0.05
Ho_2O_3	0.29	0.00–0.62	0.79	0.61–1.02	Ho	0.01	0.02
Er_2O_3	0.84	0.29–1.28	0.90	0.79–0.99	Er	0.02	0.03
Tm_2O_3	bdl		0.29	0.20–0.58	Tm	< 0.01	0.01
Yb_2O_3	1.25	0.90–1.58	1.14	0.60–1.38	Yb	0.03	0.03
Lu_2O_3	0.11	0.00–0.35	bdl		Lu	< 0.01	
(ΣLn_2O_3)	6.64		6.57		(ΣLn)	0.18	0.20
ThO_2	18.11	16.69–19.85	1.39	1.09–1.96	Th	0.37	0.03
UO_2	6.65	5.76–7.67	19.22	18.20–19.93	U^{4+}	0.13	0.42
					$\Sigma(A)$	0.96	0.99
MnO	2.34	2.07–2.65	0.97	0.83–1.17	Mn	0.18	0.08
Fe_2O_3	10.79	10.24–11.29	11.59	11.42–11.98	Fe^{3+}	0.73	0.86
					$\Sigma(M)$	0.91	0.94
TiO_2	0.90	0.80–0.99	1.95	1.58–2.43	Ti	0.06	0.15
ZrO_2	1.48	0.92–1.76	bdl		Zr	0.06	
Nb_2O_5	45.75	45.45–46.18	25.52	24.22–26.25	Nb	1.85	1.14
Ta_2O_5	1.12	0.83–1.31	25.82	24.42–27.22	Ta	0.03	0.70
WO_3	1.02	0.73–1.10	bdl		W	0.02	
Total	100.47		99.45		$\Sigma(B)$	2.02	1.99

bdl below detection limit

[a]Average of six analyses

[b]Average of five analyses

[c]Calculated on the basis of eight oxygen atoms per formula unit

with hematite. The valence of Fe in BP could not be proven using bond-valence approach because of metamict state of the mineral. However, cation bond-valence sums of recrystallized samarskite-(Y) from annealed sample BP-1100 are consistent with Fe^{3+} (see below). Since annealing was performed in inert atmosphere, this proves the presence of ferric iron in natural BP. It is to be noted that previously reported results of XAFS (Nakai et al. 1987) and Mössbauer spectroscopy (Malczewski and Grabias 2008) show that metamict samarskite-(Y) from different localities exhibits highly varying Fe^{3+}/Fe^{2+} ratios. According to the results of Malczewski et al. (2010), at least a part of divalent iron in metamict samarskite-(Y) can be attributed to reduction of Fe^{3+} to Fe^{2+} in the course of metamictization process (reduction by β-rays, i.e., free electrons). Samarskite-(Y) from the Laacher See is strongly enriched in thorium and chemically close to a hypothetic Th-dominant ($Th > \Sigma REE$) member of the samarskite group. However, because the atomic sum of $(Y + Ln) = 0.43$ prevails over that of Th (0.37 *apfu*), the mineral should be named samarskite-(Y), according to the current nomenclature for rare-earth minerals (Bayliss and Levinson 1988). The previously reported ThO_2 content in samarskite group minerals does not exceed 8 wt% (Bonshtedt-Kupletskaya 1969; Makarochkin 1982; Polyakov 2000) except for Th-rich samarskite from Ishikawa, Japan, containing 21.88 wt% ThO_2 (Shibata and Kimura 1922). Another unusual feature of samarskite-(Y) from the Laacher See is unusually low Ta content (1.12 wt% Ta_2O_5).

Unlike samarskite-(Y) from the Laacher See, the studied mineral from the Blyumovskaya Pit is highly enriched in Ta and U (Table 1). Taking into account that the Blyumovskaya Pit is the type locality for samarskite-(Y), one could expect the availability of extended chemical data in the literature covering the period of almost 180 years. However, to our surprise, the number of reported analyses is less than a dozen; all of them being wet chemical determinations of bulk samples (Rose 1847; Hermann (1856); Bonshtedt-Kupletskaya 1969; Makarochkin 1982; Polyakov 2000). Moreover, we could not retrieve any reliable information on the rare-earth composition of samarskite-(Y) from the Blyumovskaya Pit. The comparison of reported data shows that they are rather heterogeneous, with wide variations in contents of essential constituents. This observation is not unexpected in view of the fact that the vein exposed by Blumovskaya Pit is a large and highly differentiated pegmatite body (Popov and Popova 2006). It is noteworthy that the highest contents of uranium and tantalum reported by Rose (1847) make his "Uranotantal" remarkably close to samarskite-(Y) studied in this work.

X-ray crystallography and crystal structure

Single-crystal XRD study of our sample from the Laacher See resulted in the first determination of the crystal structure of samarskite-(Y): indeed, it could not be performed before because only metamict material was available. Crystallographic data and atomic coordinates for the untreated Eifel mineral (sample LS) are presented in Tables 2 and 3, respectively. The structure of samarskite-(Y) (Fig. 2), albeit relatively simple, exhibits a specific type of cation ordering previously unreported among niobates and tantalates. It can be derived from the crystal structure of wolframite (ferberite) $Fe^{2+}W^{6+}O_4$ (Fig. 2) by imposing the following changes: (1) flat layers composed of corner-sharing zigzag chains of $[WO_6]$ octahedra in wolframite are replaced by topologically identical layers of $[NbO_6]$ octahedra (Fig. 3a); (2) each second $[NbO_6]$ layer is mirrored on (001) relative to the preceding one; (3) each second layer composed of zigzag chains of $[FeO_6]$ octahedra (Fig. 3b) is replaced by the infinite perforated layer of corner-sharing $[YO_8]$ square antiprisms (Fig. 3c). The appeared layer sequence can be expressed as -$[AO_8]$-$[BO_6]$-$[MO_6]$-$[BO_6]$- leading to the general formula AMB_2O_8 in which $A = \mathbf{Y}$, *Ln*, Th, U^{4+}, Ca; $M = \mathbf{Fe^{3+}}$, Mn^{2+};

Table 2 Crystal parameters, data collection and structure refinement details for samarskite-(Y)

Sample	LS[a]	LS-1100[a]	BP-1100[b]
Primary state	Crystalline	Crystalline	Metamict
Thermal treatment	Untreated (natural)	Annealed at 1100 °C	Annealed at 1100 °C
Structure refinement	Single crystal	Single crystal	Rietveld method
Crystal size (mm)	0.07 × 0.05 × 0.05	0.15 × 0.10 × 0.05	Powder sample
Crystal system; space group	Monoclinic; *P2/c*	Monoclinic; *P2/c*	Monoclinic; *P2/c*
a (Å)	9.8020 (8)	9.8006 (3)	9.7035 (4)
b (Å)	5.6248 (3)	5.6254 (2)	5.6008 (2)
c (Å)	5.2073 (4)	5.2154 (2)	5.1637 (2)
β (°)	93.406 (4)	93.481 (2)	93.285 (2)
V (Å^3)	286.59 (4)	287.01 (2)	280.17 (2)
Z	2	2	2
D_x (g cm^{-3})	6.21	6.20	6.07
Instrument	Bruker Kappa APEX II DUO	Bruker Smart APEX II	Rigaku Ultima IV
Radiation	Mo*K*α (0.71073 Å)	Mo*K*α (0.71073 Å)	Cu*K*α (1.54178 Å)
$2\Theta_{max}$ (°); R_{int} (%)	60.00; 2.14	62.00; 2.76	100.00; R_p 2.68; R_{wp} 4.28; R_{exp} 1.81
Total collected, unique and observed [$I > 2\sigma(I)$] reflections	5597; 838; 834	2982; 564; 563	
h; *k*; *l* max	13; 7; 7	12; 6; 6	9; 5; 5
R_1 [$F^2 > 2\sigma(F^2)$]; $wR_2(F^2)$ (%)	1.09; 2.76	1.59; 3.79	R_B 1.19
GooF	1.16	1.18	2.37

[a]Formula according to electron microprobe data (8 O *apfu*): $[(Y_{0.25}Ln_{0.18})_{\Sigma 0.43}Th_{0.37}U^{4+}_{0.13}Ca_{0.03}]_{\Sigma 0.96}(Fe^{3+}_{0.73}Mn^{2+}_{0.18})_{\Sigma 0.91}(Nb_{1.85}Ti_{0.06}Zr_{0.06}Ta_{0.03}W_{0.02})_{\Sigma 2.02}O_8$

[b]Formula calculated on the basis of site-scattering factors, taking into account electron microprobe data (8 O *apfu*): $[(Y_{0.61}Ln_{0.36})_{\Sigma 0.47}Th_{0.06}]_{\Sigma 1.03}(Fe^{3+}_{0.88}Mn^{2+}_{0.08})_{\Sigma 0.96}(Nb_{1.64}Ta_{0.24}Ti_{0.16})_{\Sigma 2.04}O_8$

Table 3 Fractional atomic coordinates and isotropic displacement parameters of samarskite-(Y)

Site[a]	*x*	*y*	*z*	U_{iso} (Å^2)
Sample LS				
A (2*f*)	0	0.26303 (3)	3/4	0.00623 (6)
M (2*e*)	1/2	0.33655 (8)	3/4	0.0065 (2)
B (4*g*)	0.73465 (2)	0.18404 (4)	0.28544 (4)	0.00585 (7)
O1 (4*g*)	0.13815 (15)	0.0643 (3)	0.4764 (3)	0.0101 (4)
O2 (4*g*)	0.13102 (15)	0.4059 (3)	0.0999 (3)	0.0106 (4)
O3 (4*g*)	0.63878 (15)	0.1207 (3)	0.5987 (3)	0.0106 (4)
O4 (4*g*)	0.61212 (16)	0.3772 (3)	0.0988 (3)	0.0120 (4)
Sample LS-1100				
A (2*f*)	0	0.26284 (5)	3/4	0.0045 (1)
M (2*e*)	1/2	0.33682 (16)	3/4	0.0052 (3)
B (4*g*)	0.73420 (3)	0.18354 (7)	0.28542 (6)	0.0039 (2)
O1 (4*g*)	0.1377 (2)	0.0641 (5)	0.4760 (5)	0.0082 (7)
O2 (4*g*)	0.1312 (3)	0.4051 (5)	0.1001 (5)	0.0093 (7)
O3 (4*g*)	0.6394 (3)	0.1208 (5)	0.5991 (5)	0.0091 (7)
O4 (4*g*)	0.6126 (3)	0.3764 (5)	0.0990 (5)	0.0104 (7)
Site[a]	*x*	*y*	*z*	B_{iso} (Å^2)
Sample BP-1100				
A (2*f*)	0	0.2686 (9)	3/4	0.3
M (2*e*)	1/2	0.3311 (19)	3/4	0.8
B (4*g*)	0.7342 (1)	0.1841 (6)	0.2853 (8)	0.3
O1 (4*g*)	0.138 (3)	0.071 (3)	0.468 (6)	0.3
O2 (4*g*)	0.143 (2)	0.426 (4)	0.094 (5)	0.3
O3 (4*g*)	0.647 (2)	0.119 (4)	0.607 (4)	0.3
O4 (4*g*)	0.610 (2)	0.392 (4)	0.097 (4)	0.3

[a]Site multiplicities and Wyckoff symbols are given in parentheses

B = **Nb**, Ta, Ti, W, Zr; (the species-defining constituents are highlighted in bold). We herein propose AMB_2O_8 lettering for the general formula of samarskite-group minerals, to keep consistency with site designations accepted for other groups of tantalo-niobates (Ercit 2005).

As a result of the layer alternation, the unit cell of samarskite-(Y) becomes doubled along the *a*-axis compared to that of wolframite structure archetype (Fig. 2). Among natural niobates and tantalates, heftetjernite $ScTaO_4$ (Kolitsch et al. 2010) and rossovskyite $Fe^{3+}NbO_4$ (Konovalenko et al. 2015) possess wolframite-type structure. The observed cation ordering in samarskite-(Y) is explainable on the basis of the crystal chemical criteria: the [AO_8] layer accommodates large-radius cations favoring eightfold coordination, whereas the octahedral [MO_6] layer accumulates smaller Fe and Mn (Tables 4, 5). The major substitution schemes in samarskite-(Y) can be represented as ${}^{B}Nb^{5+} \leftrightarrow {}^{B}Ta^{5+}$; ${}^{A}Y^{3+} \leftrightarrow {}^{A}HREE^{3+}$; ${}^{A}Ca^{2+} + {}^{A}U^{4+} \leftrightarrow 2{}^{A}(Y,Ln)^{3+}$; ${}^{A}U^{4+} + {}^{B}Ti^{4+} \leftrightarrow {}^{A}(Y,Ln)^{3+} + {}^{B}Nb^{5+}$; and probably, ${}^{A}U^{4+} + {}^{M}(Fe,Mn)^{2+} \leftrightarrow {}^{A}(Y,Ln)^{3+} + {}^{M}Fe^{3+}$. The topology of the [$AO_8$] layer in samarskite-(Y) (Fig. 3c) is identical to that of the [YO_8] layer in synthetic tellurite $Na_2Y_3Cl_3[TeO_3]_4$ (Zitzer et al. 2014) and largely resembles the topology of rather distorted [SnO_8] layer in foordite $Sn^{2+}Nb_2O_6$–thoreaulite $Sn^{2+}Ta_2O_6$ series (Ercit and Černý 1988). Bond-valence calculations (Table 5) unambiguously evidence for trivalent iron and divalent manganese in samarskite-(Y). Site occupancies derived from the structural data (Table 4) are in excellent agreement with the results of microprobe analyses (Table 1). It should be mentioned that the sum of Fe and Mn in the *M* group is slightly less than 1.0 *apfu*, according to both structural and microprobe data. The latter might indicate the possibility of incomplete occupancy (vacancies) in the *M* site. The ideal end-member formula of samarskite-(Y) can be expressed as $YFe^{3+}Nb_2O_8$. For the four other minerals related to samarskite group (Brøgger 1906; Kimura 1922; Ellsworth 1928; Palache et al. 1944; Hanson et al. 1999; Simmons et al. 2006), the simplified formulae could be derived by analogy and thus assumed as follows: $YFe^{3+}Ta_2O_8$ for yttrotantalite-(Y), $U^{4+}Fe^{2+}Nb_2O_8$ for ishikawaite, $(Ca,U^{4+})Fe^{3+}Nb_2O_8$ for calciosamarskite and $YbFe^{3+}Nb_2O_8$ for samarskite-(Yb). The alternation of layers appeared in samarskite-(Y) was not

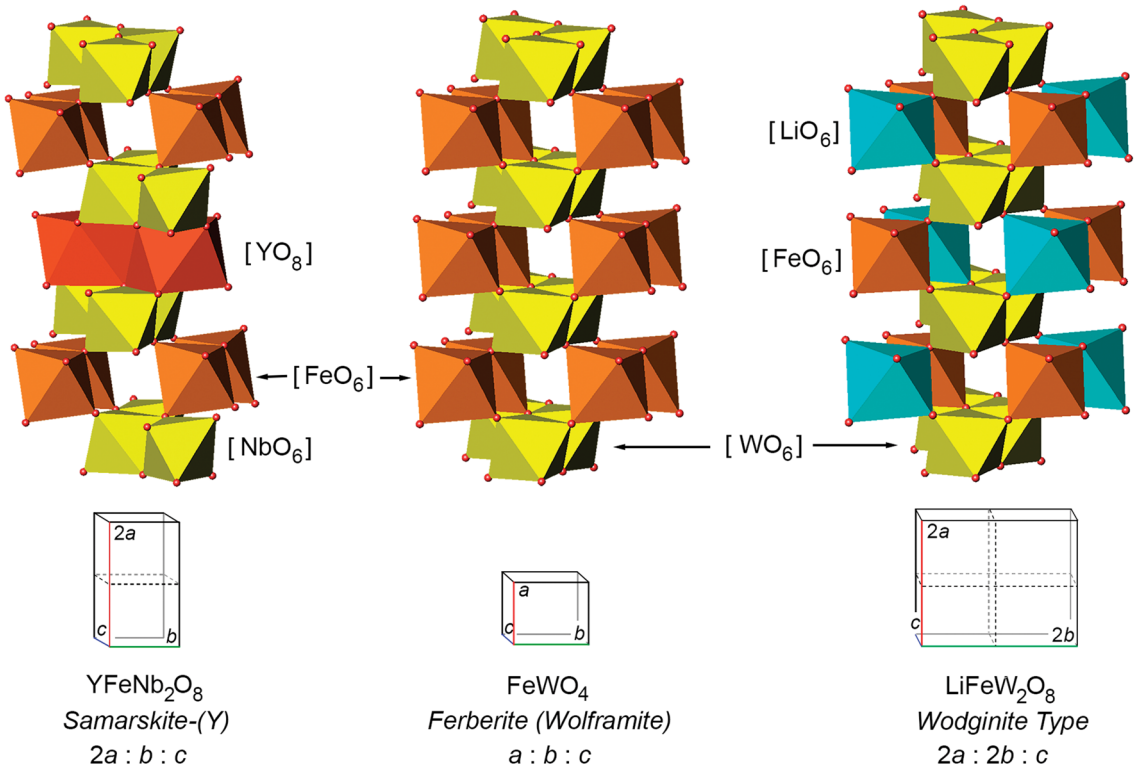

Fig. 2 Relationships between wolframite structure and its derivatives—samarskite-(Y) and $LiFeW_2O_8$ (wodginite-type structure, Albino et al. 2012). The unit cells are scaled by ½ in size and coincident with the depicted structural fragments

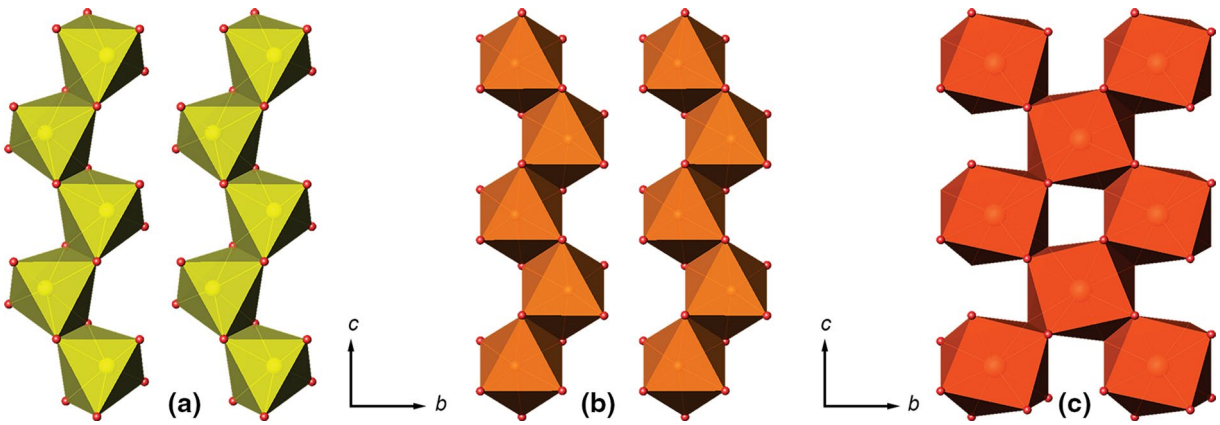

Fig. 3 Fragments of the layers in the crystal structure of samarskite-(Y). **a** Layer composed of wolframite-like zigzag chains of [NbO_6] octahedra; **b** the similar layer composed of [FeO_6] octahedra; **c** infinite perforated layer composed of edge-sharing [YO_8] square antiprisms

reported among niobates and tantalates but well represented in structurally related layered tungstates and molybdates.

The latter family is known as "double tungstates" or "double wolframites" (Le Flem et al. 1969; Maier et al. 1973). It includes numerous synthetic compounds used as phosphorescent materials and active media in solid-state lasers (Pollnau et al. 2007; Zharikov et al. 2009; Lagatsky et al. 2010). Their generalized formula can be written as $AM(W,Mo)_2O_8$. Depending on the radius of *A* and *M* cations, one can observe broad variability in their coordination environment and intralayer structures of the alternating layers (Le Flem et al. 1969; Maier et al. 1973). It should be noted, however, that in spite of overall structural similarity among compounds within the family of layered double tungstates, only one phase, the low-temperature $LiY(WO_4)_2$ (Kim et al.

Table 4 Cation site occupancies and scattering factors for samarskite-(Y)

Site	SC[a]	SOF[b]	SSF[c]	Assigned site occupancy[d]	Z[e]
Sample LS[f]					
A	Y, Th	$Th_{0.55}Y_{0.45}$	67.05	$\left(Y_{0.25}Ln_{0.18}Th_{0.37}U^{4+}_{0.13}Ca_{0.03}\right)_{\Sigma 0.96}$	67.15
M	Fe	$Fe_{0.935}$	24.31	$(Fe^{3+}_{0.73}Mn^{2+}_{0.18})_{\Sigma 0.91}$	23.48
B	Nb	$Nb_{0.969}$	39.73	$(Nb_{0.91}Ti_{0.03}Zr_{0.03}Ta_{0.02}W_{0.01})_{\Sigma 1.00}$	41.21
Sample LS-1100[f]					
A	Y, Th	$Th_{0.58}Y_{0.42}$	68.58	$\left(Y_{0.25}Ln_{0.18}Th_{0.37}U^{4+}_{0.13}Ca_{0.03}\right)_{\Sigma 0.96}$	67.15
M	Fe	$Fe_{0.940}$	24.44	$(Fe^{3+}_{0.73}Mn^{2+}_{0.18})_{\Sigma 0.91}$	23.48
B	Nb	$Nb_{0.974}$	39.93	$(Nb_{0.91}Ti_{0.03}Zr_{0.03}Ta_{0.02}W_{0.01})_{\Sigma 1.00}$	41.21
Sample BP-1100[g]					
A	Y, U	$Y_{0.75}U_{0.25}$	51.75	$(Y_{0.59}Ln_{0.35}U_{0.06})_{\Sigma 1.00}$	51.57
M	Fe	$Fe_{0.93}$	24.18	$(Fe^{3+}_{0.86}Mn^{2+}_{0.08})_{\Sigma 0.94}$	24.36
B	Nb, Ta	$Nb_{0.93}Ta_{0.07}$	43.24	$(Nb_{0.80}Ta_{0.12}Ti_{0.08})_{\Sigma 1.00}$	43.32

[a]SC, atomic scattering curves used for site occupancy refinement

[b]SOF, refined site occupancy factor

[c]SSF, refined site-scattering factor (number of electrons per site)

[d]$Ln = (Dy_{0.04}Ce_{0.03}Yb_{0.03}Nd_{0.02}Er_{0.02}La_{0.01}Sm_{0.01}Gd_{0.01}Ho_{0.01})_{\Sigma 0.18}$ based on electron microprobe data

[e]Z, mean site atomic number calculated from electron microprobe data

[f]Samples LS and LS-1100 originate from the same crystal and, therefore, have the same assumed site occupancies

[g]$Ln = (Dy_{0.09}Yb_{0.06}Er_{0.05}Ho_{0.04}Sm_{0.03}Gd_{0.03}Nd_{0.02}Tm_{0.02}Ce_{0.01})_{\Sigma 0.35}$

Table 5 Selected bond lengths (Å) and their multiplicities, bond-valence sums (BVS, v.u.) and cation site charges for samarskite-(Y)

Bond	LS		LS-1100		BP-1100	
	Length × mult.	BVS	Length × mult.	BVS	Length × mult.	BVS
A—O1	2.3116 (15) × 2	1.11	2.313 (3) × 2	1.11	2.31 (3) × 2	0.94
A—O1	2.5343 (15) × 2	0.61	2.530 (3) × 2	0.62	2.55 (2) × 2	0.49
A—O2	2.3101 (15) × 2	1.12	2.311 (3) × 2	1.12	2.36 (3) × 2	0.82
A—O2	2.4181 (16) × 2	0.84	2.424 (3) × 2	0.82	2.37 (2) × 2	0.80
Total BVS charge		3.68		3.67		3.05
Site charge[a]		3.35		3.35		3.06
M–O3	2.0181 (16) × 2	1.01	2.023 (3) × 2	1.00	2.03 (2) × 2	0.97
M–O4	2.0791 (16) × 2	0.86	2.083 (3) × 2	0.85	2.06 (2) × 2	0.89
M–O4	2.1268 (17) × 2	0.75	2.132 (3) × 2	0.74	2.06 (2) × 2	0.89
Total BVS charge		2.62		2.59		2.75
Site charge[a]		2.55		2.55		2.74
B—O1	2.0172 (15) × 1	0.75	2.023 (3) × 1	0.73	1.96 (3) × 1	0.86
B—O1	2.2045 (15) × 1	0.45	2.208 (3) × 1	0.45	2.24 (3) × 1	0.40
B—O2	1.8854 (15) × 1	1.07	1.885 (3) × 1	1.07	1.89 (2) × 1	1.04
B—O3	2.1583 (16) × 1	0.51	2.152 (3) × 1	0.52	2.09 (2) × 1	0.91
B—O3	1.9630 (16) × 1	0.86	1.962 (3) × 1	0.87	1.94 (2) × 1	0.60
B—O4	1.8515 (16) × 1	1.17	1.844 (3) × 1	1.19	1.90 (2) × 1	1.01
Total BVS charge		4.80		4.82		4.82
Site charge[a]		4.95		4.95		4.92

[a]Total charge of cation site based on the assumed site occupancy (Table 4). Bond valence sums were calculated based on parameters reported by Brese and O'Keefe (1991)

2006), possesses structural motif which almost exactly replicates the samarskite one.

Samarskite-(Y) has the same general formula as wodginite-group minerals, $AM(Ta,Nb,Ti)_2O_8$ (Ferguson et al. 1976; Ercit et al. 1992; Galliski et al. 2016); however, they are principally different in terms of crystal chemistry. Wodginite-type compounds do not contain large cations, such as *REE*, Ca, Th or U, and both *A* and *M* sites in their structures are octahedrally coordinated. The appearance of $2a \times 2b$ superlattice in wodginites is achieved via intralayer octahedral cation ordering (Fig. 2).

Thermal transformations

State of the art

A review of early references related to thermal treatment of metamict samarskite was given by Nilssen (1970). Komkov (1965) was the first who assigned XRD pattern of the phase formed upon heating of samarskite in air to 660 °C to wolframite-type structure. Sugitani et al. (1984, 1985) showed that annealing of metamict samarskite in reducing atmosphere (5% H_2/95% Ar) leads to consecutive formation of two phases: first, a low-temperature phase appeared at 550–700 °C which gradually transforms to the high-temperature modification above 950 °C (Table 6). The low-temperature form is either monoclinic ($\beta \sim 90°$) or orthorhombic and thus related to wolframite (Fe, Mn)WO_4 or ixiolite (Ta, Mn, Nb, Fe, Sn)O_2 (= α-PbO_2) structure type, respectively. Structural nature of the high-temperature form (with doubled unit-cell volume) was not resolved, although Warner and Ewing (1993) suggested its relationship to $NaFeW_2O_8$ which belongs to double tungstates (Klevtsov and Klevtsova 1970). Note that Warner and Ewing (1993) have exchanged the positions of *a* and *b* axes in samarskite unit cell reported by Sugitani et al. (1985). It should be pointed out, however, that such $a \leftrightarrow b$ interchange is a crystallographically forbidden operation in monoclinic system (with unique axis *b*), as the *b* axis is interlocked with the position of monoclinicity plane and β angle. A comparison of published data (Table 6) revealed that Komkov (1965) applied correct (wolframite-type) unit-cell setting for low-temperature form, whereas Sugitani et al. (1985) and succeeding authors interchanged $a \leftrightarrow b$ axes in the unit cells of both forms. The latter raised some questions about the quality of published XRD data. That is, along with the lack of reliable thermal data on samarskite-(Y) from the type locality, inspired us to perform TG-DSC study followed by XRD examination of the mineral from both the Laacher See (LS) and the Blyumovskaya Pit (BP). Contrary to Sugtani et al. (1984, 1985), high-purity argon atmosphere was used for the preservation of original oxidation state of Fe and U.

Table 6 Unit-cell settings and parameters of samarskite-(Y) reported by different authors

Space group	*a* (Å)	*b* (Å)	*c* (Å)	β (°)	References
Low-temperature form					
P2/c	4.82 (1)	5.63 (1)	5.15 (1)	~90	Komkov (1965)
P2/c	4.830 (3)	5.645 (3)	5.162 (3)	90.42 (1)	This work, BP-700-1[a]
Pbcn (?)	**5.687 (4)**	**4.925 (2)**	5.210 (4)	90.02 (8)	Sugitani et al. (1984)
Pbcn (?)	4.774	5.740	5.068		Sugitani et al. (1985)[b]
Pbcn	**5.68 (1)**	**4.94 (1)**	5.24 (2)		Tomašić et al. (2010)
n.r.[c]	**5.66 (1)**	**4.910 (6)**	5.19 (1)	90.4 (2)	Akimoto et al. (1986)
High-temperature form					
P2/c	9.8020 (8)	5.6248 (3)	5.2073 (4)	93.406 (4)	This work, natural LS
P2/c	9.8006 (3)	5.6254 (2)	5.2154 (2)	93.481 (2)	This work, LS-1100
P2/c	9.7035 (4)	5.6008 (2)	5.1637 (2)	93.285 (2)	This work, BP-1100
P2/c	**5.642 (7)**	**9.914 (8)**	5.229 (3)	93.84 (7)	Sugitani et al. (1985)
n.r.[c]	**5.638**	**9.90**	5.230	93.88	Sugitani et al. (1985)[b]
n.r.[c]	**5.714 (11)**	**9.931 (13)**	5.217 (19)	93.47 (20)	Hanson et al. (1999)
n.r.[c]	**5.688 (9)**	**9.915 (2)**	5.199 (9)	93.16 (10)	Simmons et al. (2006)[d]
P2/c	**5.626 (1)**	**9.918 (2)**	5.249 (1)	93.92 (1)	Tomašić et al. (2010)

[a]Phase BP-700-1 as refined in monoclinic setting (wolframite structure type) for comparison with the data by Komkov (1965) Orthorhombic (ixiolite) setting accepted in this work is given in Table 7

[b]Synthetic product

[c]Space group was not reported

[d]Samarskite-(Yb). Incorrectly defined (interchanged $a \leftrightarrow b$) parameters are highlighted in bold. Estimated standard deviations are given in parentheses

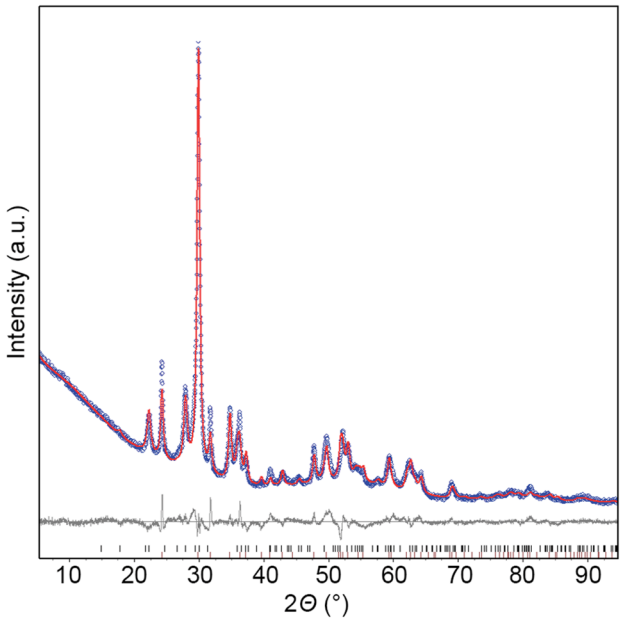

Fig. 4 Rietveld refinement plot for the sample BP-700. Experimental profile is traced by blue circles; calculated pattern is shown as red line; difference curve as gray line. Two rows of vertical bars denote the positions of Bragg reflections corresponding to the phases BP-700-1 and PB-700-2, respectively (see Table 7)

Samarskite-(Y) from the Laacher See

Annealing of crystal fragment of samarskite-(Y) for 40 h at 1100 °C did not affect its crystal structure: samples LS and LS-1100 possess almost identical unit-cell parameters and structural characteristics (Tables 2, 3, 4, 5). The results of Rietveld refinement of finely ground crystals (Table S1 in Supplementary material) confirm that both LS and LS-1100 are single-phase samples with the unit-cell metrics identical to those determined by single-crystal XRD study.

Samarskite-(Y) from the type locality

Heating of metamict sample BP from the Blyumovskaya Pit to 1100 °C (experiment T2 in "Samples and methods" section) resulted in flat TG line (weight change < 0.1 wt%) and a single exothermic event at 645 °C (Fig. S1 in Supplementary material). The latter is attributed to recrystallization of metamict material; the peak position is consistent with the data reported by Komkov (1965) (660 °C) and later authors (550–750 °C, references are listed in Table 6). The negligible value of weight change evidences for (1) lack of chemically significant water content and (2) the absence of thermal events related to oxidation of either Fe or U. The latter allows assuming that oxidation states of iron and uranium determined by bond-valence calculations for the heat-treated samples BP-700 and BP-1100 are the same as in the original metamict samarskite-(Y). The results of full-profile Rietveld refinement of sample BP-700 (metamict samarskite heated to 700 °C) are presented in Fig. 4 and summarized in Table 7. The sample consists of two phases. The dominant one, BP-700-1 (84 wt%), corresponds to the "low-temperature form" of samarskite first recognized by Komkov (1965). Because of poor crystallinity of the sample and hence broad XRD peaks, refinement in either monoclinic (wolframite-type, $P2/c$, $Z=2$, Table 6) or orthorhombic setting (α-PbO_2-type, $Pbcn$, $Z=4$, Table 8) gives virtually indistinguishable fit results. We herein accept the low-symmetry, orthorhombic setting. Refined site occupancies, bond-valence sums and charge balance (Table 8) are in agreement with the formula $\left[Nb_{0.30}Fe^{3+}_{0.30}(Y,Ln)_{0.15}Ta_{0.15}U^{4+}_{0.10}\right]_{\Sigma 1.00}O_2$. This phase exhibits disordered distribution of cations within the single

Table 7 Rietveld refinement details and phase composition of sample BP-700

Phase name	BP-700-1	BP-700-2
Formula[a]	$\left[Nb_{0.30}Fe^{3+}_{0.30}(Y,Ln)_{0.15}Ta_{0.15}U^{4+}_{0.10}\right]_{\Sigma 1.00}O_2$	$U_{1.00}(Nb_{0.76}Ta_{0.24})_{\Sigma 1.00}Ta_{2.00}O_{10}$
Structure type	α-PbO_2	UNb_3O_{10}
Crystal system	Orthorhombic	Orthorhombic
Space group	*Pbcn*	*Fddd*
a (Å)	4.829 (3)	7.39 (3)
b (Å)	5.642 (3)	12.80 (5)
c (Å)	5.161 (3)	15.980 (9)
V (Å^3)	140.6 (1)	1511 (9)
Z	4	8
D_x (g cm^{-3})	6.83	6.80
Phase content (wt%)	84 (2)	16 (2)
R_B (%)	1.31	1.83

Thermal experiment T3 in "Samples and methods" section. R_p 2.21; R_{wp} 3.19; R_{exp} 1.94%; *GooF* 1.65

[a](Y,*Ln*) = $(Y_{0.64}Dy_{0.10}Yb_{0.06}Er_{0.05}Ho_{0.04}Sm_{0.03}Gd_{0.03}Nd_{0.02}Tm_{0.02}Ce_{0.01})_{\Sigma 1.00}$ according to electron microprobe analysis of untreated BP sample (Table 1)

Table 8 *M* site properties and interatomic bond distances for phase BP-700-1

Property	Value
SC	Fe, Ta
SOF	$Fe_{0.53}Ta_{0.47}$
SSF	48.09
Assigned site occupancy	$Nb_{0.30}Fe^{3+}_{0.30}(Y, Ln)_{0.15}Ta_{0.15}U^{4+}_{0.10}$
Z	47.49
$d(M—O)^{i}$ (Å)	1.946 (8) × 2
$d(M—O)^{ii}$ (Å)	2.060 (8) × 2
$d(M—O)^{iii}$ (Å)	2.242 (7) × 2
Bond-valence charge	3.89
Formula charge	4.00

Fractional atomic coordinates and isotropic displacement parameters: site *M* (4*c*) $x=0$; $y=0.1943(3)$; $z=¼$; $B_{iso}=3.6$ Å^2. Site O (8*d*) $x=0.2711(16)$; $y=0.4145(16)$; $z=0.3912(13)$; $B_{iso}=3.6$ Å^2

SC atomic scattering curves used for site occupancy refinement, *SOF* refined site occupancy factor, *SSF* refined site-scattering factor (number of electrons per site), *Z* mean site atomic number calculated on the basis of assigned site occupancy. Bond-valence sums were calculated taking parameters reported by Brese and O'Keefe (Brese and O'Keefe 1991)

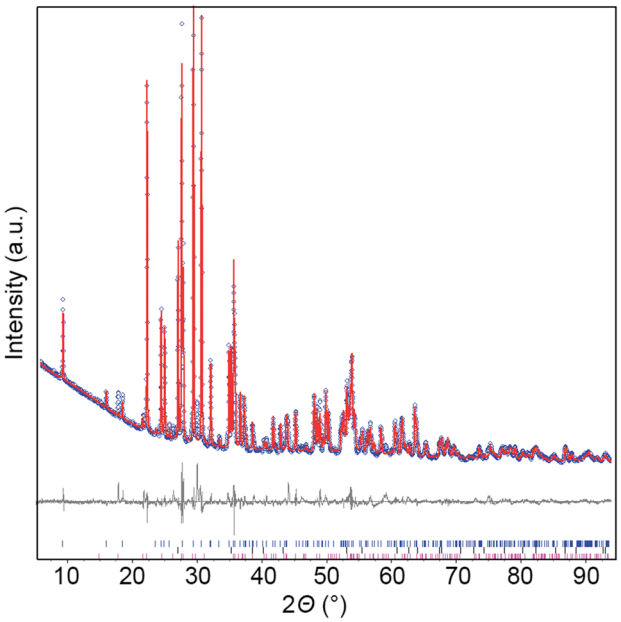

Fig. 5 Rietveld refinement plot for the sample BP-1100. R_p 2.68; R_{wp} 4.28; R_{exp} 1.81%; *GooF* 2.37. Experimental profile is traced by blue circles; calculated pattern is shown as red line; difference curve as gray line. Three rows of vertical bars denote the positions of Bragg reflections corresponding to (1) Samarskite-(Y), 65 wt%, R_B 1.19% (Tables 2, 3, 4, 5); (2) $FeTaO_4$ (rutile structure type, $P4_2/mnm$), 12 wt%, R_B 1.26%; (3) $U(Ta,Nb)_3O_{10}$, 23 wt%; R_B 1.23%

octahedral *M* site and can be regarded as "ashanite", or a Nb-dominant analogue of ixiolite $(Ta,Mn,Nb,Fe,Sn)O_2$ (Grice et al. 1976). The second, subordinate phase, BP-700-2 (Table 7), is a Ta-dominant counterpart of synthetic compound UNb_3O_{10} (Miyake et al. 1987). It is important that this compound contains pentavalent but not hexavalent uranium (Miyake et al. 1987) meaning, in due course, that oxidation state of uranium in metamict samarskite did not exceed U^{5+}. The occurrence of U^{5+} in primordial samarskite from the Blyumovskaya Pit cannot be ruled out (see, for instance, Skomurski et al. 2011), provided that a part of ferric iron (Table 1) should then be inverted to ferrous one. However, comparison with crystalline samarskite from the Laacher See (Table 1) suggests that the latter scenario is unlikely to occur. It cannot be excluded that partial $U^{4+}Fe^{3+} \rightarrow U^{5+}Fe^{2+}$ charge redistribution could take place during the annealing process. The emergence of UNb_3O_{10}-like phase can be explained by inability of octahedral *M* site of ixiolite structure to accommodate 15 wt% of uranium contained in the metamict samarskite. The excess of U is thus damped out into $U(Ta,Nb)_3O_{10}$. However, for the majority of metamict samarskites which contain 5–8 wt% of U, demetamictization at 700 °C can really yield single ixiolite-like phase (Komkov 1965; Sugitani et al. 1984, 1985 and others). That does not mean, however, the structure of this compound corresponds to the original, pre-metamict samarskite state. Instead, according to the Ostwald's rule of stages (Ostwald 1897; Van Santen 1984), such first appearing phase typically represents a transitional, quickly crystallizing polymorph.

Long-time annealing of ixiolite-like phase at 1100 °C (experiment T4 in "Samples and methods" section) leads to its partial decomposition and transformation into the final, stable samarskite-(Y) structure. For the purposes of comparison, crystallographic and structural data for this newly formed samarskite-(Y) (sample BP-1100) are grouped together with the data on the mineral from the Laacher See (Tables 2, 3, 4, 5). Site occupancies in the structure of this re-appeared samarskite-(Y) could be recalculated with good accuracy assuming that it does not contain uranium (Table 4), resulting in the structural formula $\left(Y_{0.59}Ln_{0.35}Th_{0.06}\right)_{\Sigma 1.00}\left(Fe^{3+}_{0.86}Mn^{2+}_{0.08}\right)_{\Sigma 0.94}\left(Nb_{1.60}Ta_{0.24}Ti_{0.16}\right)_{\Sigma 2.00}O_{8.00}$. High-temperature form of samarskite constitutes the main part of BP-1100 sample (Fig. 5). The remaining 35 wt% are divided between $U(Ta,Nb)_3O_{10}$ and rutile-type $FeTaO_4$. It should be emphasized, however, that neither one of the phases formed upon recrystallization of metamict samarskite-(Y) from the type locality represents its original, pre-metamict structural state.

Summarizing the results of studies of samarskite-(Y) from the Laacher See and the type locality (the Blyumovskaya Pit), one can state that so-called "high-temperature" form of the mineral represents the only stable modification of this niobate. The appearance of a metastable ixiolite(or wolframite)-type phase upon heating of a metamict mineral obeys Ostwald's rule of stages (Ostwald 1897; Van Santen

1984) indicating that this "low-temperature" form is a transitional but most quickly crystallizing intermediate. The exact pathways of thermal behavior of metamict samarskite-group minerals are largely dependent on their chemical composition and degree of secondary alteration (hydration and selective leaching of chemical constituents) and never result in complete restoring of original, pre-metamict crystalline phase.

Conclusions

The results of present work offer samarskite-(Y) as a first member of a new family of layered niobates and tantalates. It is important that samarskite-(Y) can be synthesized using simple sintering approach (Sugitani et al. 1984); therefore, one can expect that the new cation-substituted samarskites can be synthesized as well. Following multiple fields of applications realized in synthetic Nb- and Ta-based oxides, samarskite structure can be used as a novel oxide template in materials science. The obtained results could provide new insights on the mineralogy and petrology of the samarskite group in general. The crystal chemical criteria unambiguously explain well-known trends in preferable accumulation of Th, U and *REE* in samarskite but not in chemically similar wolframite and wodginite group minerals. Like other metamict phases, samarskite-(Y) resisted the attempts to reveal its primordial, pre-metamict structural state for a long time. It looks obvious that many reported occurrences of samarskite-like niobates may in fact represent either heavily altered (hydrothermal or weathered) mineral or just other metamict minerals resembling samarskite by the set of principal chemical constituents (Ercit 2005; Capitani et al. 2016). In either case, these metamict phases (or any associated inclusions embedded in these phases) cannot be unambiguously ascribed to the primary mineral. Therefore, a great care should be taken prior making any conclusions regarding original structural state of metamict minerals. The results of present work could be considered crystal chemical base which substantiates recently reported statistical data on the chemistry of samarskite-group minerals (Kjellman 2017). The latter study shows that the majority of chemical analyses of samarskite correspond to a stoichiometry AMB_2O_8. Therefore, our results, along with the statistical data by Kjellman (2017), provide the basement for the new nomenclature of samarskite group, based on the ordered formula AMB_2O_8.

Acknowledgements S.N.B and M.G.K thank Saint-Petersburg State University for financial support (Grant No. 3.42.741.2017). The authors thank the X-ray Diffraction Center of SPSU for providing instrumental and computational resources. We acknowledge Radek Škoda and Giancarlo Capitani for constructive reviews and discussion. We are also grateful to Milan Rieder for the editorial handling of the manuscript.

References

Akimoto J, Uejima A, Sugitani Y (1986) Studies on annealing conditions for recovering the original samarskite structure. Kobutsugaku Zasshi 17:159–168 **(in Japanese)**

Albino M, Pechev S, Veber P, Velazquez M, Josse M (2012) Cation ordering in the double tungstate $LiFe(WO_4)_2$. Acta Crystallogr C68:i7–i8

Baales M, Joris O, Street M, Bittmann F, Weninger B, Wiethold J (2002) Impact of the late glacial eruption of the Laacher See volcano, Central Rhineland, Germany. Quat Res 58:273–288

Bayliss P, Levinson AA (1988) A system of nomenclature for rare earth mineral species: revision and extention. Am Mineral 73:422–423

Bonshtedt-Kupletskaya EM (1969) Samarskite. In: Chukhrov FV, Bonshtedt-Kupletskaya EM (eds) Minerals, II (3) (complex oxides, titanates, niobates, tantalates, antimonates, hydroxides). Nauka, Moscow, pp 331–339 **(in Russian)**

Bräuer K, Kämpf H, Niedermann S, Strauch G (2013) Indications for the existence of different magmatic reservoirs beneath the Eifel area (Germany): a multi-isotope (C, N, He, Ne, Ar) approach. Chem Geol 356:193–208

Brese NE, O'Keefe DM (1991) Bond-valence parameters for solids. Acta Crystallogr B47:192–197

Britvin SN, Dolivo-Dobrovolsky DV, Krzhizhanovskaya MG (2017) Software for processing the X-ray powder diffraction data obtained from the curved image plate detector of Rigaku RAXIS rapid II diffractometer. Proc Russ Mineral Soc 146(3):104–107

Brøgger WC (1906) Die Mineralien der Südnorwegischen Granitpegmatitgänge. I. Niobate, Tantalate. Titanate und Titanoniobate. Skrift Matem-Natur Klasse 6:138–151

Bruker (2003) SAINT (ver. 7.60A). Bruker AXS Inc, Madison

Bruker (2014) TOPAS, Version 5.0. Bruker AXS Inc, Madison

Capitani GC, Mugnaioli E, Guastoni A (2016) What is the actual structure of samarskite-(Y)? A TEM investigation of metamict samarskite from the Garnet Codera dike pegmatite (Central Italian Alps). Am Mineral 101:1679–1690

Cassedanne JP, Baptista A, Černý P (1985) Zircon hafnifère, samarskite et columbite d'une pegmatite du Rio Doce, Minas Gerais, Brésil. Can Mineral 23:563–567

Černý P, London D, Novák M (2012) Granitic pegmatites as reflections of their sources. Elements 8:289–294

Chukanov NV, Aksenov SM, Rastsvetaeva RK, Belakovskiy DI, Göttlicher J, Britvin SN, Möckel S (2012a) Christofschäferite, $(Ce, La, Ca)_4Mn^{2+}(Ti, Fe^{3+})_3(Fe^{3+}, Fe^{2+}, Ti)(Si_2O_7)_2O_8$, a new chevkinite-group mineral from the Eifel area, Germany. New Data Miner 47:33–42 **(in Russian)**

Chukanov NV, Blass G, Pekov IV, Belakovskiy DI, Van KV, Rastsvetaeva RK, Aksenov SM (2012b) Perrierite-(La), $(La, Ce, Ca)^4Fe^{2+}(Ti, Fe)_4(Si_2O_7)_2O_8$, a new mineral species from the Eifel volcanic district, Germany. Geol Ore Depos 54:647–655

Chukanov NV, Blass G, Zubkova NV, Pekov IV, Pushcharovskii DYu, Prinz H (2013) Hydroxymanganopyrochlore: a new mineral from the Eifel Volcanic Region, Germany. Dokl Earth Sci 449(1):342–345 **(in Russian)**

Chukanov NV, Krivovichev SV, Pakhomova AS, Pekov IV, Schäfer Ch, Vigasina M, Van K (2014) Laachite, $(Ca, Mn)^2Zr^2Nb^2TiFeO_{14}$, a new zirconolite-related mineral from the Eifel volcanic region, Germany. Eur J Mineral 26:103–111

Della Ventura G, Bellatreccia F, Williams CT (2000) Zirconolite with significant $REEZrNb(Mn, Fe)O_7$ from a xenolith of the Laacher See eruptive center, Eifel volcanic region, Germany. Can Mineral 38:57–65

Demarçay E-A (1901) Sur un nouvel élément l'europium. Compt Rend 132:1484–1486

Dill HG (2015) Pegmatites and aplites: their genetic and applied ore geology. Ore Geol Rev 69:417–561

Dolomanov OV, Bourhis LJ, Gildea RJ, Howard JA, Puschmann H (2009) OLEX2: a complete structure solution, refinement and analysis program. J Appl Crystallogr 42:339–341

Donakowski MD, Görne A, Vaughey JT, Poeppelmeier KR (2013) J Am Chem Soc 135:9898–9906

Ellsworth HV (1928) A mineral related to samarskite from the Woodcox Mine, Hybla Ontario. Am Mineral 13:63–65

Engelhaupt B, Schüller W (2015) Samarskit-(Y). In: Engelhaupt B, Schüller W (eds) Mineral Reich Eifel. Christian Weise Verlag, München, p 249

Ercit TS (2005) Identification and alteration trends of granitic-pegmatite-hosted (Y, REE, U, Th)-(Nb, Ta, Ti) oxide minerals: a statistical approach. Can Mineral 43:1291–1303

Ercit TS, Černý P (1988) The crystal structure of foordite. Can Mineral 26:899–903

Ercit TS, Černý P, Hawthorne FC, McCammon CA (1992) The wodginite group. II. Crystal chemistry. Can Mineral 30:613–631

Ewing RC (1975) The crystal chemistry of complex niobium and tantalum oxides. IV. The metamict state: discussion. Am Mineral 60:728–733

Ferguson RB, Hawthorne FC, Grice JD (1976) The crystal structures of tantalite, ixiolite and wodginite from Bernic Lake, Manitoba. II. Wodginite. Can Mineral 14:550–560

Galliski MA, Márquez-Zavalía MF, Černý P, Lira R, Roberts AC, Bernhardt H-J (2016) Achalaite, $Fe^{2+}TiNb_2O_8$, a new member of the wodginite group from the La Calandria granitic pegmatite, Córdoba, Argentina. Can Mineral 54:1043–1052

Grice JD, Ferguson RB, Hawthorne FC (1976) The crystal structure of tantalite, ixiolite and wodginite from Bernic Lake, Manitoba. I. Tantalite and ixiolite. Can Mineral 14:550–560

Grigor'ev DP (1945) Regular intergrowth of samarskite and columbite from the Ilmeny Mountains. Zap Vsesoyuzn Mineral Obsch 74:57–61 **(in Russian)**

Hanson SL, Simmons WB Jr, Falster AU (1998) Nb–Ta–Ti oxides in granitic pegmatites from the Topsham pegmatite district, southern Maine. Can Mineral 36:601–608

Hanson SL, Simmons WB, Falster AU, Foord EE, Lichte FE (1999) Proposed nomenclature for samarskite-group minerals: new data on ishikawaite and calciosamarskite. Mineral Mag 63:27–36

Hermann R (1856) Untersuchungen über Niobium. J Prakt Chem 68:65–97

Keller C (1962) Über ternäre Oxide des Niobs und Tantals vom Typ ABO_4. Z Anorg Allg Chem 318:89–106

Kim JS, Lee JC, Cheon CI, Kang H-J (2006) Crystal structures and low temperature cofiring ceramic property of $(1–x)(Li, RE)W_2O_8$-$xBaWO_4$ ceramics (RE = Y, Yb). Jpn J Appl Phys 45:7397–7400

Kimura K (1922) Ishikawaite: a new mineral from Ishikawa, Iwaki. J Geol Soc Tokyo 29:316–320 **(in Japanese)**

Kjellman J (2017) ABC_2O_8—a new look on the crystal chemistry and classification of samarskite group minerals. In: PEG2017: proc. 8th int. symp. granitic pegmatites, pp 64–67

Klevtsov PV, Klevtsova RF (1970) Single-crystal synthesis and investigation of the double tungstates $NaR^{3+}(WO_4)_2$, where R^{3+} = Fe, Sc, Ga and In. J Solid State Chem 2:278–282

Kolitsch U, Kristiansen R, Raade G, Tillmanns E (2010) Heftetjernite, a new scandium mineral from the Heftetjern pegmatite, Tørdal, Norway. Eur J Mineral 22:309–316

Kolitsch U, Mills SJ, Miyawaki R, Blass G (2012) Ferriallanite-(La), a new member of the epidote supergroup from the Eifel, Germany. Eur J Mineral 24:741–747

Komkov AI (1965) Crystal structure and chemical composition of samarskite. Dokl Acad Sci USSR Earth Sci Sect 160:127–129

Konovalenko SI, Ananyev SA, Chukanov NV, Rastsvetaeva RK, Aksenov SM, Baeva AA, Gainov RR, Vagizov FG, Lopatin ON, Nebera TS (2015) A new mineral species rossovskyite, $(Fe^{3+}, Ta)(Nb, Ti)O^4$: crystal chemistry and physical properties. Phys Chem Miner 42:825–833

Lagatsky AA, Han X, Serrano MD, Cascales C, Zaldo C, Calvez S, Dawson MD, Gupta JA, Brown CTA, Sibbett W (2010) Femtosecond (191 fs) $NaY(WO^4)^2$ Tm, Ho-codoped laser at 2060 nm. Opt Lett 35:3027–3029

Le Flem G, Salmon R, Hagenmuller P (1969) Cation distribution in an ordered wolframite-type structure. Compt Rend Acad Sci C 268:1431–1434

Lecoq de Boisbaudran P-É (1879) Recherches sur le samarium, radical d'une terre nouvelle extradite de la samarskite. Compt Rend Acad Sci 89:212–214

Lecoq de Boisbaudran P-É (1886) Le Yα de M. de Marignac est dèfinitivement nomme gadolinium. Compt Rend Acad Sci 102:902

Maier AA, Provotorov MV, Balashov VA (1973) Double molybdates and tungstates of the rare earths and alkali metals. Russ Chem Rev 42:822–833

Makarochkin BA (1982) Chemical composition of accessory titano-tantalo-niobates of Ilmen Mountains. U.S.S.R. Academy of Sciences, Sverdlovsk **(in Russian)**

Malczewski D, Grabias A (2008) ^{57}Fe Mössbauer spectroscopy and X-ray diffraction study of complex metamict minerals. Part II. Hyperfine Interact 186:75–81

Malczewski D, Grabias A, Dercz G (2010) ^{57}Fe Mössbauer spectroscopy of radiation damaged samarskites and gadolinites. Hyperfine Interact 195:85–91

Marignac MC (1880) Sur les terres de la samarskite. Ann Chim Phys 20:535–557

Miyake C, Ohana S, Imoto S (1987) Oxidation states of U and Nb in U–Nb–O ternary oxides by means of magnetic susceptibility, XPS and ESR. Inorg Chim Acta 140:133–135

Nakai I, Akimoto J, Imafuku M, Miyawaki R, Sugitani Y, Koto K (1987) Characterization of the amorphous state in metamict silicates and niobates by EXAFS and XANES analyses. Phys Chem Mineral 15:113–124

Nilssen B (1970) Samarskites. Chemical composition, formula and crystalline phases produced by heating. Norsk Geol Tidsskr 50:357–373

Ostwald W (1897) Studien über die Bildung und Umwandlung fester Koerper. Z Phys Chem 22:289–330

Palache C, Berman H, Frondel C (1944) The system of mineralogy of James Dwight Dana and Edward Salisbury Dana Yale University 1837–1892, volume I: elements, sulfides, sulfosalts, oxides, 7th edn. Wiley, New York

Papoutsa AD, Pe-Piper G (2013) The relationship between REE-Y-Nb-Th minerals and the evolution of an A-type granite, Wentworth Pluton, Nova Scotia. Am Mineral 98:444–462

Pekov IV (1998) Minerals first discovered on the Territory of the Former Soviet Union. OP, Moscow

Pieczka A, Szuszkiewicz A, Szełęg E, Ilnicki S, Nejbert K, Turniaiak K (2014) Samarskite-group minerals and alteration products: an example from the Julianna pegmatitic system, Piława Górna, SW Poland. Can Mineral 52:303–319

Pollnau M, YaE Romanyuk, Gardillou F, Borca CN, Griebner U, Rivier S, Petrov V (2007) Double tungstate lasers: from bulk toward on-chip integrated waveguide devices. IEEE J Select Top Quantum Electron 13:661–671

Polyakov VO (2000) Samarskite. In: Yushkin NP (ed) Mineralogy of urals. Oxides and hydroxides. Part. I. Branch of Russian Academy of Sciences, Miass-Yekaterinburg **(in Russian)**

Polyakov VO, Zhdanov VF, Nishanbaev TP (1980) New receipts of the museum of the Ilmeny state reserve. In: Mineralogicheskie issledovaniya gidrotermalitov Urala, Sverdlovsk, pp 52–58 **(in Russian)**

Popov VA, Popova VI (2006) Ilmeny Mountains: mineralogy of pegmatites. In: Mineralogical almanac, vol 9. Association Ecost and Ocean Pictures Ltd, Littleton, p 151

Popov VA, Popova VI, Polyakov VO (2007) Regular intergrowths of minerals in pegmatites from the Il'meny Mountains. Geol Ore Depos 49:573–582

Rose G (1839) Beschreibung einiger neuen Mineralien des Urals. Ann Phys 124(12):551–573

Rose H (1847) Ueber die Zusammensetzung des Uranotantals und des Columbits vom Ilmengebirge in Sibirien. Ann Phys 147(5):157–169

Scheldrick GM (2015) Crystal structure refinement with *SHELXL*. Acta Crystallogr C71:3–8

Shibata Y, Kimura K (1922) Chemical investigation of Japanese minerals containing rarer elements. IV. Samarskite and an unnamed mineral from Ishikawa, Iwaki Province. Nippon Kagaku Kaishi 43:301–312

Simmons WB, Hanson SL, Falster AU (2006) Samarskite-(Yb): a new species of the samarskite group from the Little Patsy pegmatite, Jefferson County, Colorado. Can Mineral 44:1119–1125

Skomurski FN, Ilton ES, Engelhard MH, Arey BW, Rosso KM (2011) Heterogeneous reduction of U^{6+} by structural Fe^{2+} from theory and experiment. Geochim Cosmochim Acta 75:7277–7290

Sugitani Y, Suzuki Y, Nagashima K (1984) Recovery of the original samarskite structure by heating in a reducing atmosphere. Am Mineral 69:377–379

Sugitani Y, Suzuki Y, Nagashima K (1985) Polymorphism of samarskite and its relationship to other structurally related Nb-Ta oxides with the α-PbO_2 structure. Am Mineral 70:856–866

Tomašić N, Gajović A, Bermanec V, Linarić MR, Su D, Škoda R (2010) Preservation of the samarskite structure in a metamict ABO_4 mineral: a key to crystal structure identification. Eur J Mineral 22:435–442

Uher P, Ondrejka M, Konečny P (2009) Magmatic and post-magmatic Y-REE-Th phosphate, silicate and Nb-Ta-Y-REE oxide minerals in A-type metagranite: an example from the Turčok massif, the Western Carpathians, Slovakia. Mineral Mag 73:1009–1025

Van Santen RA (1984) The ostwald step rule. J Phys Chem 88:5768–5769

Warner JK, Ewing RC (1993) Crystal chemistry of samarskite. Am Mineral 78:419–474

Zharikov EV, Zaldo C, Díaz F (2009) Double tungstate and molybdate crystals for laser and nonlinear optical applications. MRS Bull 34:271–276

Zitzer S, Schleifenbaum F, Schleid T (2014) $Na_2Y_3Cl_3[TeO_3]_4$: synthesis, crystal structure and spectroscopic properties of the bulk material and its luminescent Eu^{3+}-doped samples. Z Naturforsch B 69:150–158

Publisher's Note Springer Nature remains neutral with regard to jurisdictional claims in published maps and institutional affiliations.